Scholar Publishing Group
International Journal of Engineering Technology and Construction
https://doi.org/10.38007/IJETC.2022.030403
ISSN 2789-7176 Vol. 3, Issue 4: 28-42

Combined Sensor Method for Measuring Torsional Vibration and Anti-Collapse Performance of Steel Frame under Strong Earthquake

Radhakrishna Ramyam*

LBEF Campus, Nepal

**corresponding author*

Keywords: Structural Torsional Vibration, Combined Sensor, Shock-Absorbing Steel Frame, Strong Earthquake Action, Collapse Resistance

Abstract: As the main torque sensor for real-time monitoring work, its development is of great significance to people. People use torque sensors to monitor and control torque in real time, which is critical to ensure the safe operation of the test system. This research is mainly to use the combined sensor method to measure the torsional vibration of the structure and analyze the anti-collapse performance of the shock-absorbing steel frame under strong earthquake. Experimental data shows that the limit bending moment of JD01 without end plate reinforcement is 130.7 kN m, while the limit bending moment of end plate reinforcement is 160.7 kN m. Compared with JD01, the bending ability of JD02 has increased by 22.95%. The results of the study show that the configuration of the reinforcing material of the bottom plate can effectively alleviate the stress concentration problem of the bottom plate, limit the surface deformation of the bottom plate, improve the rotation capacity of the node, and improve the support capacity of the node. The buckling restraint support can act as a reverse member of the elastic stage, supporting part of the horizontal shear force. The elastoplastic stage effectively adjusts the reverse side rigidity of the floor, adjusts the shear distribution of the floor, reduces the shear value of each layer, and finally delays the main bearing member to enter the elastic stage.

1. Introduction

Due to the increasing scarcity of urban space resources and the continuous development of building technology, high-rise buildings are on the rise. Society has gradually entered the era of information and intelligence, and the rapid development of sensors has made our production and life more comfortable and convenient. Using the combined sensor method to measure the angular vibration of the structure can determine the speed, load and working state of the measured

Copyright: © 2022 by the authors. This is an Open Access article distributed under the Creative Commons Attribution License (CC BY 4.0), which permits unrestricted use, distribution, and reproduction in any medium, provided the original work is properly cited (https://creativecommons.org/licenses/by/4.0/).

mechanism, and use simulation analysis to analyze trends and predict accidents. In recent years, earthquakes have occurred frequently in various places, which has caused great problems to people's production and life, and people's requirements for earthquake resistance and earthquake resistance of buildings have become higher and higher. In the seismic design and anti-seismic consolidation of new and old buildings, energy consumption and impact buffer devices are continuously used. As a new type of energy-absorbing shock absorber, the anti-buckling brace can provide lateral rigidity to the structure during small earthquakes, and it can also generate hysteretic energy consumption after retreating during large earthquakes.

This study combines the combined sensor to measure the torsional vibration of the structure, and analyzes the damping effect and the collapse resistance of the building under the strong earthquake action of the steel frame. Using nonlinear finite structural analysis, a multi-layer space frame structure model was developed, and the method of dismantling elements was used to analyze the continuous collapse resistance of the structure, and the continuous collapse performance at different stages under vertical load resistance was analyzed to find improved buildings The direction of the ability of the object to resist collapse.

Today, torque measurement technology has become a new branch of measurement technology, and torque measurement is also a basic element of various mechanical product development, quality testing, optimization, condition inspection and fault diagnosis. Berke believes that the ASTM E1875 acoustic resonance method is a convenient method to obtain the properties of elastic materials, especially at high temperatures. This technique is performed by exciting a rectangular test strip to vibrate in a certain frequency range while measuring its vibration amplitude. At a specific frequency, the local maximum of the displacement amplitude indicates deflection or torsional resonance. The elastic modulus and shear modulus are then calculated based on the first flexural and torsional resonance frequencies and the mass and size of the rod, respectively. However, for some strip geometries, the order in which different resonance frequencies appear depends on the Poisson's ratio of the material [1]. Although this method can quickly learn the characteristics of elastic materials, its accuracy is relatively low. Li proposed a novel method based on fiber Bragg grating (FBG) sensing for analyzing and separating the coupled bending and torsional vibrations of the rotating shaft. He derived a theoretical strain detection model based on FBG, which was carried out under pure torsional vibration and coupled bending and torsional vibration. Two FBG sensors have been installed on opposite sides of the rotating shaft at an angle of 45° relative to the axial direction to support the use of the proposed decoupling method and determine the decoupled bending and torsion signals. He designed a new support device to protect the optical fiber rotary joint from damage under heavy load impact and ensure stable signal transmission. The calibration sensitivity of the measured torque of the attached FBG is 7.02pm/Nm. Dynamic experiments have been carried out on the rotor platform at different speeds to effectively decouple bending and torsional strains in real time [2]. The results of his experimental data are more comprehensive, but the operation is more complicated. Xiu-Kun described and studied a method for monitoring spindle bending and torsional vibration in CNC machining tools. This method uses the Doppler frequency shift of the laser beam, more specifically, the differential method of two parallel beams and Mach-Zehnder heterodyne interference to measure the axle vibration. The mixed interference signal is measured with a photoelectric detector. By using frequency discrimination, the transient speed can be decoupled from the torsional vibration of the machine tool [3]. Although his method is theoretically feasible, it is difficult to use and has many variables.

This study establishes a nonlinear finite element fiber model for a self-controlled energy failure support structure system. Through the use of different performance indicators, the effect of the self-failure device on the seismic resistance of the structure was evaluated, and the condition of structural damage was evaluated based on the performance evaluation indicators. By installing

sensors on the elastic shaft for experiment and analyzing the relative maximum error, the ultimate goal of nonlinear correction for dual sensors can be achieved.

2. Combined Sensor to Measure Torsional Vibration Structure

2.1. Combined Sensor Data Fusion

Combined sensor is a technology that collects and represents different data, and at the same time can stimulate the internal connection between the data to optimize the data. The data fusion technology of combined sensors has many advantages: improve the reliability of the system, expand the coverage of the system, improve the reliability of the integrated data and the response speed of the system, avoid the redundancy and Contradictions reduce uncertainty [4].

Electric strain measurement and sensor technology mainly have the following advantages. The resistance strain gauge is small, lightweight, and easy to install, and generally does not interfere with the stress distribution of the component. High measurement sensitivity, high precision, and wide range: Generally speaking, under the condition of small strain, the special large strain gauge can reach a maximum of 40,000 micro strain [5]. The minimum grid length of the strain gauge at room temperature is within the measurable stress concentration range, and the frequency response is high. The use of electronic devices for automation, remote measurement, transmission of electrical signals, digital display, printing, and data processing. Various types of sensors are made of resistance strain gauges and special elastic elements, which can measure physical quantities such as force, load, pressure, torque, displacement, acceleration, etc. with an accuracy of up to 0.5% to 0.01% [6].

The process of multi-sensor data fusion is shown in Figure 1. The specific steps are divided into data collection, pre-processing, calculation, output, etc. [7].

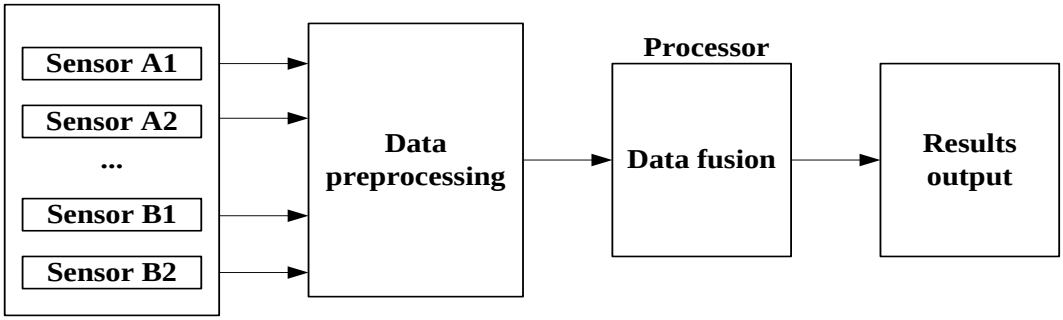

Figure 1. Multi-sensor data fusion process

The structure of data fusion can be divided into three forms: serial, parallel and mixed.

(1) Serial. The current sensor needs to obtain the output of the previous sensor as fusion data. When the output of the previous sensor is wrong, the subsequent fusion is invalid [8].

(2) Parallel connection. Each sensor sends its output information directly to the multi-sensor data Fusion center without affecting each other [9].

(3) Mixed. Combining the first two fusion methods, the construction of hybrid Fusion is more complicated, but Fusion has strong capabilities and excellent fault tolerance [10].

2.2. Torsional Vibration Measurement Technology

Rotary spring vibration measurement methods include laser Doppler method, deflection measurement torque measurement method, angular acceleration measurement method and pulse vibration measurement method based on encoder disc [11].

(1) Pulse timing vibration measurement method

The pulse positioning mode mainly uses devices (optical rotating gears or encoders, etc.) and sensors (Hall sensors, electromagnetic sensors, capacitive sensors, etc.) that can rotate with the measuring axis and whose angle is correctly encoded [12]. Measure the torsional vibration using reflective fiber sensors, etc. When the angular slope of the encoder disk (gear tip, etc.) passes through the sensor probe, the sensor emits a corresponding pulse [13]. When the encoder disk rotates with the measuring shaft, the sensor emits a series of pulses accordingly. The processing of the pulse sequence provides information about the torsional vibration of the shaft system.

The elastic shaft will deform after twisting, and stress and strain will occur on the shaft. On the inclined surface of the shaft surface of $45°$ and $135°$ of the shaft, it bears vertical stress. This vertical stress is the principal stress, and its value is the same as the shear stress of the section. The stress body is stretched and compressed in the opposite direction [14]. Maximum tensile stress σ_1 and compressive stress σ_1 and $\sigma_1 = -\sigma_2 = \tau_{\max}$. According to the strain of the material mechanics along the strain gauge R1 direction and R2 direction ε_1, ε_2 are:

$$\varepsilon_1 = \frac{\sigma_1}{E} - v\frac{\sigma_2}{E} = \frac{1}{E}(\sigma_1 - v\sigma_2) \quad (1)$$

$$\varepsilon_2 = \frac{\sigma_2}{E} - v\frac{\sigma_1}{E} = \frac{1}{E}(\sigma_2 - \sigma_1) \quad (2)$$

In the formula, v represents Poisson's ratio and E represents the elastic modulus [15].

Because $\sigma_1 = -\sigma_2$, it is organized:

$$\varepsilon_1 = \frac{\sigma_1}{E}(1+v) = -\varepsilon_2 \quad (3)$$

From the working principle of the strain gauge, we can know that $\frac{\Delta R}{R} = K\varepsilon$, so

$$M = \frac{C_0}{KR}\Delta R = C_2 \Delta R \quad (4)$$

(2) Distortion torque measurement method

The torsional vibration measurement method of the distortion gauge adopts the method of contact measurement, the resistance strain gauge array is pasted on the shaft system to be measured, and the external circuit is connected with the slip ring lead [16]. The resistance value of the resistance strain gauge is calculated by measuring the resistance value, the deformation information of the rotating shaft is analyzed and calculated, the power spectrum of the shaft system is obtained, and the torsional vibration of the shaft system is analyzed based on the obtained power spectrum.

2.3. Shaft Model

At present, the shaft system used to calculate the torsional vibration of the shaft system can be roughly divided into three categories: simple mass model, multi-level mass model and continuous mass model [17]. A simple block mass model can accurately represent the low-order torsional vibration characteristics of the shaft system. The equation order is low and the calculation amount is small, but the model is relatively simple and the model order is too low to reflect the high-frequency mode in the model. The multi-segment mass model is a multi-mass spring system. The number is usually 30-300, which can accurately reflect the low-order and high-order rotational vibration characteristics, but its calculation accuracy is affected by the number of boxes. Continuous mass models have various types of shaft systems that can be accurately described, and can simply calculate the force of the shaft system on any cross-section [18]. The simplified model is close to

the actual system, but the calculation of the model is complicated, and it is difficult to apply to the real-time simulation of the system. The calculation method of the forced vibration based on the model is difficult to realize. When establishing a continuous mass model of shaft torsional vibration, people often perform discrete and degraded processing on it. Generally, there are two ways to reduce the order of models. One method is to reduce the order of accurate higher-order models, and the other is to identify the system through shaft operation and test data, and then establish a method of lower-order models [19].

3. Steel Frame Shock Absorption System and Anti-Collapse Performance

3.1. Shock Absorption System

The impact absorption control classification of engineering structures is shown in Figure 2. Starting from the relationship between the source and the vibration system, the following methods can be used for the seismic resistance of the building structure: one is to suppress the generation of the source, that is to say reduce the vibration strength of the source, and the other is vibration insulation, that is, vibration insulation Set between the source and the vibration system, the device is used to separate vibrations. Third, it is mainly to reduce the vibration of the vibration system [20]. The main purpose is to install vibration damping devices in the vibration control system for energy control and dynamic vibration absorption [21].

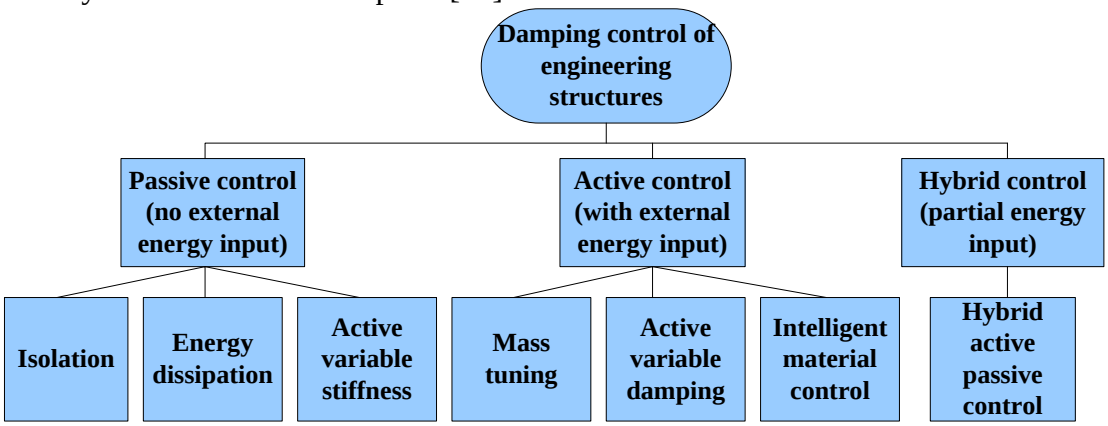

Figure 2. Classification of shock absorption control

The advantages of steel structure:

(1) Lightweight, high strength, good plastic toughness. The strength of steel is much higher than other materials, and the weight is lighter, which is especially suitable for large-span or high-load structures [22]. Good plastic toughness makes it have large deformation capacity without brittle failure and strong adaptability to dynamic load, which is very suitable for earthquake-resistant structural systems such as wind resistance and earthquake resistance [23].

(2) The material is uniform and more consistent with the assumptions of machine computing. Because the steel is uniform and has few defects, it is consistent with the assumption of mechanical calculations that can easily perform theoretical calculations and analysis. At the same time, the agreement with the material model in numerical simulation is high, and the reliability of the results is high [24].

3.2. Anti-Buckling Restraint Support

Reverse buckling restraint blades are also called buckling beam blades and non-joint blades, and are mainly composed of a core unit, a restraint unit, and a sliding mechanism unit. The thickness of

the steel plate of the core unit is usually 10 to 80 mm. Constraint factors need to have sufficient bending stiffness to ensure adequate restraint under action conditions and prevent buckling from restricting the support from local buckling [25]. In addition, it is also necessary to confirm that the local coupling will not fail or buckle to prevent restraint support connection nodes or splice failures [26]. The slider unit is a non-bonded material filled on the boundary surface between the inner side of the restraint unit and the core unit. The main purpose is to provide sufficient axial deformation space for the anti-buckling constraint of the operating state to support the core element, so that the mechanical state of the core element is basically the same under the action of tension and pressure [27].

The relationship expression of core concrete $\sigma-\varepsilon$ in steel tube is as follows:

$$y=\begin{cases}2\cdot x-x^2(x\le 1)\\ \dfrac{x}{\beta_0\cdot(x-1)^{\eta}+x}(x>1)\end{cases} \quad (5)$$

$$\begin{cases}x=\dfrac{\varepsilon}{\varepsilon_{c0,CFST}}\\ y=\dfrac{\sigma}{\sigma_{c0,CFST}}\end{cases} \quad (6)$$

$$\begin{cases}\varepsilon_{c0,CFST}=\varepsilon_c+800\cdot\xi^{0.2}\cdot 10^{-6}\\ \sigma_{c0,CFST}=f_c'(N/mm^2)\end{cases} \quad (7)$$

$$\xi=\frac{f_yA_s}{f_{ck}A_c} \quad (8)$$

$\sigma_{c0,CFST}$ is the peak stress of the stress-strain ratio, $\varepsilon_{c0,CFST}$ is the strain force corresponding to the peak stress, f_y and f_{ck} are the yield strength and compressive strength of the steel pipe in the core area, A_s and A_c are the cross-sectional areas in the steel pipe and concrete of the core area [28].

3.3. Seismic Performance

(1) Static elastoplasticity

In the static elastoplastic analysis method of a structure or component, a certain force is first applied to the vertical axis, then the horizontal force is added in the form of adding a specific distribution or horizontal displacement, and then gradually increasing until the structure or component is destroyed is the ideal state ,Modeling. Parts or low loads, plastic hinge formation, and other failure conditions occur during load cycles at various levels, and the performance index [29]. In order to find the weak position, damage mechanism and failure mode of the structure or component, evaluate the elastoplastic performance to study the structure or component and determine whether the structure or component meets the load or deformation specifications. The calculation flow chart is shown in Figure 3.

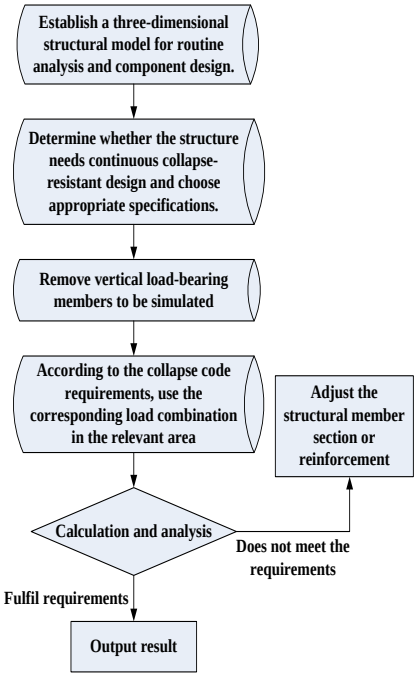

Figure 3. Static elastoplastic calculation process

(2) Finite element model

Commonly used static elastoplastic analysis models are:

1) Mid-level model: the mass of the structural particles is concentrated in each floor, and the vertical lateral force against each floor member is combined into a member, and the function of this member is reflected by the so-called "equivalent rigidity between floors" Thus, a series of rigid plate system models are formed, which have obvious advantages in the analysis of floor parameters and the study of macroscopic laws of structural seismic response [30].

2) Rod model. The basic element of the analysis is composed of beams and columns in the frame. The mass is concentrated at the node level, and each node has independent degrees of freedom. The model can obtain the local internal force and the deformation state of each bar, reflecting the changes in structural strength, stiffness and mass, as well as the difference in the order and degree of failure between each bar of the frame in the inelastic period.

3) Solid model. According to the physical force state of the element, the area is divided, and the analysis result is more accurate, but this method is computationally intensive, inefficient, and uneconomical.

3.4. Collapse Resistance

Methods for analyzing the continuous collapse of structures are divided into two categories:

1) Analysis of unexpected loads. The incremental power analysis method can gradually adjust the intensity value of seismic records (or multiple seismic records) to create one or more sets of records with amplified intensity, and perform nonlinear dynamic time analysis on each seismic intensity record until the structure Until it collapses. The IDA curve links the seismic intensity parameters and corresponding structural response parameters. At the same time, it can determine the overall structural requirements or seismic capacity [31].

2) Analysis of local damage. Assuming that the structure was initially destroyed and one or more elements of the structure were removed, then the propagation and structure of the initial failure were analyzed. The resistance to continuous collapse is determined by the frequency of normal collapse or other unexpected loads.

4. Steel Frame Pseudo-Static Test

4.1. Steel Frame Production

The size of the test project was reduced to 1:3 to produce a two-layer steel tube composite concrete frame with a height of 1555 mm and 1650 mm, and the length of the frame was 3000 mm. The first and second layers of the frame are connected at the ends by expandable end plates and flush end plates. M20 single-sided bolts are installed at the joints of the nodes, and the end of the bolts is welded with 80mm long threaded steel to enhance the anchoring performance between the bolts and the concrete in the center of the steel column. The test model parameters are shown in Table 1.

Table 1. Model parameters

Model number	Number of layers	Storey height(mm)	Column section(mm)	Beam section(mm)	End plate type
SCF	First layer	1555	2000	250×6	Flush out
	Second layer	1650			
CCF	First layer	1555	2000	250×6	Flush out
	Second layer	1650			

4.2. Loading Device

(1) Vertically applied load: Place the top of the test element column on a 1000 kN hydraulic cylinder, the axial pressure ratio is 0.3, and the axial force simulates a vertical load.

(2) Horizontal loading: the hydraulic servo actuator is fixed on the reaction force wall, and the actuator applies horizontal thrust to the west side bearing plate of the frame.

First pre-load the test elements to check the test and loading system. Then apply a load, observe the measuring instrument used to record the initial reading, and perform the previous horizontal displacement on the upper part of the loading frame. Make two observations on the measuring point channel at each loading stage to ensure that all constraints are observed, all displacements and all rotation angles change linearly with increasing load, if the unloading is zero, all values will return to the first reading.

4.3. Test Phase

In order to determine the relative angular displacement of the beam node and the lateral displacement of the chassis column, the displacement device is mainly arranged at the upper end of the beam and the right end of the bottom beam.

(1) Displacement measurements in the horizontal direction of A1, A2 and A3 are arranged at the axis of the first and second layer steel beam frame columns respectively to measure the lateral displacement of the frame columns.

(2) Three vertical spoilers A4, A5 and A6 are respectively arranged on the steel layer to measure the rotation and bending between the two ends of the steel layer, and three vertical spoilers A7, A8 and A9 are arranged in the second The rotation and bending of the end of the steel beam of the second layer are measured on the steel beam of the second layer.

(3) The horizontal offsets A10 and A11 are arranged on the west side of the cylinder and cooperate with the vertical offsets A6 and A9 to make the beam fall on the ends of the first and second layers, and then measure the rotation angle.

(4) Rebar tension: Place 12 stress plates on the longitudinal reinforcement of the first and second floor concrete floors.

(5) Bolt stress: Two stress plates are buried on the bolts in the first and second floor reinforced concrete floors.

5. Anti-Collapse Performance Analysis

5.1. Analysis of the Relationship between Load and Displacement

(1) As the displacement increases, the interlayer shear force and base shear force of the test piece SCF1 increase, and the gradient of the curve decreases. If the load is applied in the same direction at the same level, the gradient of the second load curve will decrease. The decrease in the rigidity of the structure accelerates as the load increases. The interlayer shear force and basic shear force of CCF1 increase with the increase of displacement. When the load is applied in the same direction at the same level, the gradient of the two load curves is similar, and the rigidity decline is not obvious.

(2) Comparison of interlayer shear between specimen SCF1 and specimen CCFr. Apex displacement and basic shear displacement between available layers: hysteresis curve of specimen CCF1 load, small crisis, early slow load curve is still intact, specimen SCF1 is slightly mixed, the energy performance of its circular steel tube concrete composite frame, repair concrete filling The rectangular steel tube frame is better. The area of the hysteresis loop of the test piece SCF1 is larger than that of the test piece CCF1, showing that the energy consumption of the square concrete-filled steel tube composite frame is larger than that of the round concrete-filled steel tube composite frame.

(3) The area of the hysteresis loop of the first layer of the test piece is larger than that of the second layer, and the energy consumption of the protruding end plate connected composite frame is greater than that of the flat plate connected composite frame.

5.2. Finite Element Analysis

The results of finite element analysis are shown in Table 2. The end plate reinforcement material JD01 of the limit bending moment is not 130.7kN ṁ, and the end plate reinforcement material of the limit bending moment is 160.7kN ṁ. The bending support force of JD01 is increased by 22.9% compared to JD02, and it can be seen that the end plate reinforced material group can effectively relieve the stress. In order to improve the concentration phenomenon of the end plate and the rotation ability of the node, limit the out-of-plane deformation of the end plate and increase the supporting force of the node. The maximum bending moment of JD03 is 15.5kN ṁ, which is 17.44% higher than that of JD01 node. According to the curve of the angle relationship of bending moment, when the thickness of the end plate is increased, the initial rotational rigidity of the joint will be slightly increased. If the thickness of the base plate is increased, the increase in the supporting force of the node is limited. When the thickness of the end plate is greater than the thickness of the column edge, the end column edge breaks earlier than the end plate. Therefore, in the seismic design of building structures, the reasonable choice of the thickness of the bottom plate can first effectively avoid the damage of the structural columns and meet the ductile design requirements of "strong columns and weak beams".

As shown in Figure 4, the end plate connection nodes have good retention characteristics and the duration of the nodes is better. Especially in JD05 with column vent acceleration ribs, the deformation of the outer surface of the top plane of the column is limited by the acceleration ribs, making it The plastic deformation is fully exerted, so the end plate acceleration ribs and column vent acceleration ribs allow the nodes of the column to effectively absorb seismic energy through

the end plates connected to the ribs.

Table 2. Analysis results of node finite element method

Node number	Unidirectional loading		Initial rotation stiffness (kN ·m / mrad)
	Ultimate load / kN	Ultimate bending moment / kN ·m	
JD01	108.2	130.7	11.02
JD02	133.2	160.7	14.01
JD03	128.2	153.5	12.25
JD04	132.8	161.2	13.46
JD05	157.4	188.7	18.22

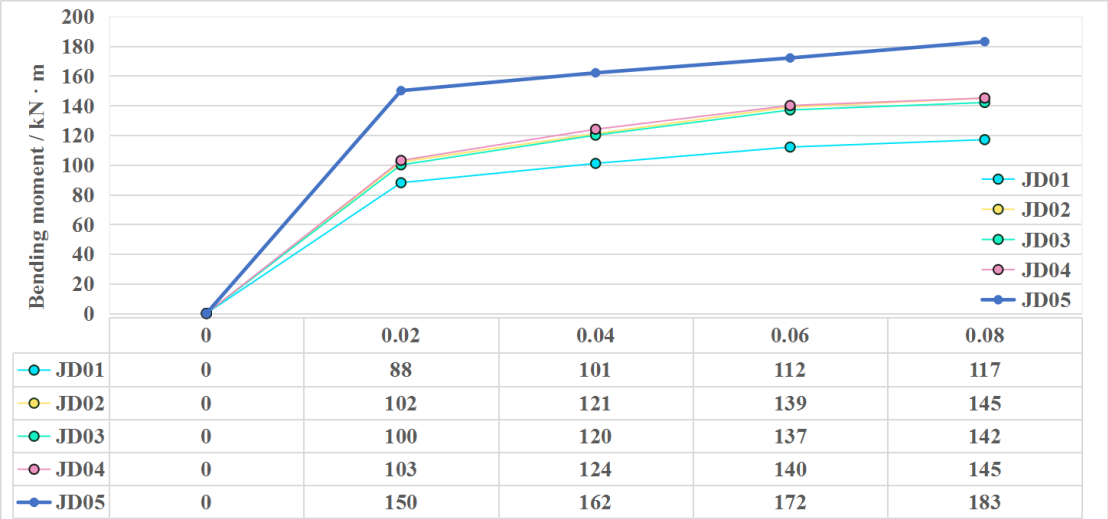

	0	0.02	0.04	0.06	0.08
JD01	0	88	101	112	117
JD02	0	102	121	139	145
JD03	0	100	120	137	142
JD04	0	103	124	140	145
JD05	0	150	162	172	183

Figure 4. Relationship between bending moment and angle

5.3. Analysis of Dynamic Characteristics of Model Structure

Table 3 shows the damping frequency and natural frequency of the structure at various positions after the seismic wave enters. The damping ratio and frequency of the model gradually increase with the strengthening of seismic intensity. Earthquake input seismic action and self-vibration damping frequency are reduced, which means that the stiffness of the model structure decreases as the input seismic action increases.

Table 3. Model natural frequency and damping ratio

White noise serial number	1	2	3	4	5	6	7	8	9	10
Frequency / Hz	6.563	6.557	6.546	6.524	6.494	6.471	6.46	6.398	6.321	6.235
Damping ratio /%	3.22	3.29	3.36	3.48	3.61	3.71	3.75	3.94	4.18	4.45

The acceleration magnification coefficient curves of each layer of the model are shown in Figure 5. In any case, as seismic excitation increases, the acceleration amplification factor has the same trend for different layers, with similar amplitude changes. At the same time, except in some cases, the amplification factor of the acceleration of each layer decreases with the intensity of the seismic wave, which indicates that the damage of the structure increases with the increase of the seismic intensity, and the lateral horizontal stiffness decreases.

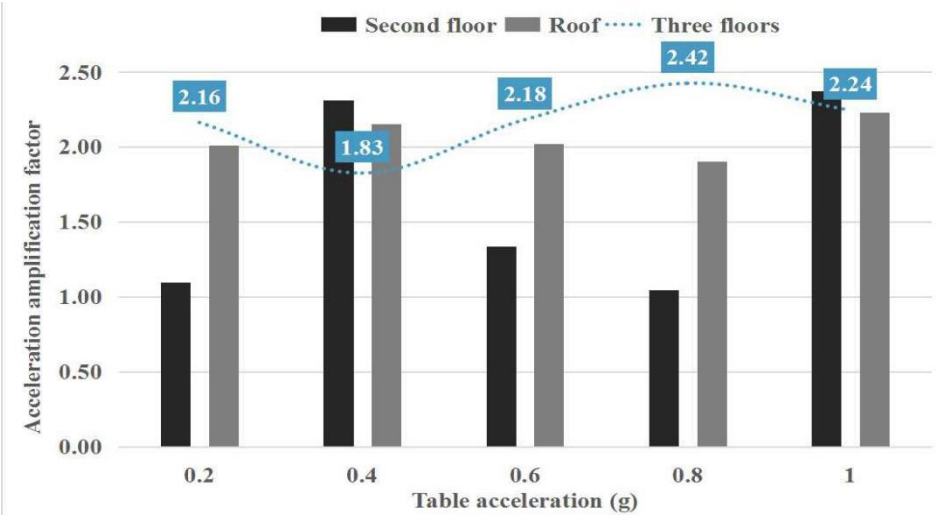

Figure 5. Acceleration coefficients for each layer of the model

5.4. Analysis of the Influence of Component Failure Location

After removing the side column, inner column and center column, the vertical curves at the top and corners of the column are shown in Figure 6. When the upper column is removed, due to the absence of vertical columns, the maximum value of the transverse tension beam causes excessive deformation of the structure, the angular displacement of the beam-column joint is the largest, the dynamic response is strongest, and the bearing capacity is completely lost; the upper inner column is removed When compared with the upper middle column, the vertical movement time curves of the two are relatively close; when the second layer side column is removed, the angular displacement of the connection between the beam column and the inner column after removal is slightly larger than that of the middle column. The vertical deflection amplitude of the top of the structural column is slightly larger than that of the inner column and the center column, an increase of about 26%, while the angle adjustment range of the balcony joint is significantly larger than that of the inner column and the center column, an increase of about 668%. When the inner column and the middle column are removed, the vertical displacement time history curve of the column top is close to the curve of the corner, and the displacement is also similar.

Figure 6. Relationship between the vertical displacement time history curve of the column top and the node angular displacement time history

The analysis shows that the dynamic response of the structure caused by the sudden damage of

the side column is much larger than that of the inner column and the side column, and the force between the inner column and the middle column is close. Therefore, the dynamic response of the inner column and the center column is very close. In frame structures with different spans and cross-sectional dimensions, the dynamic effects of component failures vary depending on the structural dimensions. Furthermore, the dynamic response of the structure is greatest when the uppermost side column is damaged. This is after the topmost side column is destroyed, the structure partially loses the vertical force transmission path, and causes large deformation or the collapse of part of the structure. In the case of a three-dimensional steel frame structure, the stresses of the side columns and prisms will become more complicated. Therefore, in the structural design, a multi-channel standby power transmission path is formed around the side columns and angle constraints. If the side columns and corner columns change suddenly due to accidental loads, adding components will increase the redundancy of the structure, adjust the structure of the internal force to adjust the stress of the residual structure more reasonably, and may also cause column damage under dynamic loads. The collapse may even cause local severe structural damage.

As shown in Figure 7, if the initial displacement is small and in the yield stage, the energy dissipation of the CFST reinforced composite wall is almost the same as the normal wall; as the displacement gradually increases, the effect of CFST appears. Under the same displacement, CFST The energy dissipation of the reinforced composite wall is significantly higher than that of the ordinary concrete wall; and as the displacement increases, the gap increases. When the initial displacement control is small, the energy loss coefficients of Q1 and Q2 are smaller than P1 and P2. This is because the energy dissipation difference between the CFST composite wall and the ordinary lattice concrete wall is small during this period, but at the same displacement, the bearing capacity of the CFST composite wall is relatively large, thereby reducing the ratio.

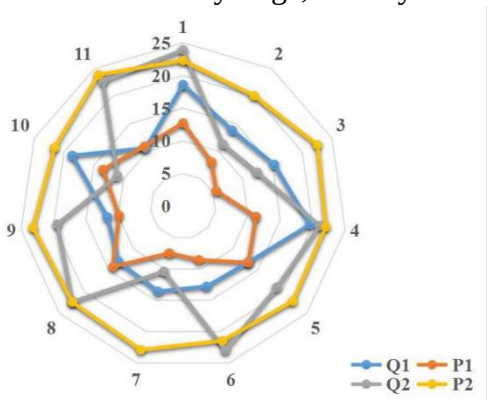

Figure 7. Comparison of dissipation coefficients of test pieces

6. Conclusion

This study is mainly based on the composite sensor method to determine the torsional vibration of the structure and the collapse resistance of the steel frame that is attenuated by the strong earthquake. By changing the direction of the resistance strain gauge, the error caused by the bending moment during torque measurement can be reduced, and the non-linear correction uses the curve fitting method to improve the measurement accuracy. In the elastic phase, the anti-buckling constrained brace can act as an anti-transverse member to bear part of the lateral shear force. In the elastic-plastic stage, effectively adjust the floor lateral rigidity, adjust the distribution of floor shear force, reduce the shear value of each floor, and finally delay the application of the main stress components to reduce the elasticity.

The damage position of the component parts has different effects on the dynamic response of the

structure. In a flat steel frame structure, the side column that causes structural dynamic response damage is usually larger than the internal cylinder and side column. Only after the damage load of the upper frame beam and the column connected by the bear, the suspension mechanism cannot be formed, and the structure will be greatly deformed. Therefore, it is necessary to strengthen the angle limitation of the side column and the periphery and improve the structure of continuous collapse resistance.

As the supporting force and elastic stiffness of the joint increase, the total energy consumption of the composite frame increases. The total input of the structure is not affected by the attenuation ratio. As the attenuation ratio of the structure increases, the ratio of lag energy consumption to total energy consumption gradually decreases. The main reason is that as the structure attenuation ratio increases, the attenuation energy consumption increases, and the lag energy consumption decreases. The historical energy dissipation of the multi-layer semi-rigid concrete filled steel tube (CFST) composite frame structure under vibration is not evenly distributed in the vertical direction. The lag energy consumption of the structure is vertically distributed according to the trapezoidal rule, the lag energy consumption of the lower part is the largest, and the upper part is the smallest.

Funding

This article is not supported by any foundation.

Data Availability

Data sharing is not applicable to this article as no new data were created or analysed in this study.

Conflict of Interest

The author states that this article has no conflict of interest.

References

[1] Berke R B , Walter M E . Using Specimen Geometry to Isolate Flexural and Torsional Vibration Modes During Sonic Resonance. Journal of Testing & Evaluation, 2016, 44(1):121-127.https://doi.org/10.1520/JTE20140016

[2] Li T , Shi C , Tan Y , et al. Fiber Bragg Grating Sensing-Based Online Torque Detection on Coupled Bending and Torsional Vibration of Rotating Shaft. Sensors Journal, IEEE, 2017, 17(7):1999-2007.https://doi.org/10.1109/JSEN.2017.2669528

[3] Xiu-Kun Y , Xiao-Qi T , Guo-Lu M A . Real-time monitoring of the flexural and torsional vibration of the main axle of a numerically-controlled machine tool. Journal of Optics, 2017, 46(3):352-357.https://doi.org/10.1007/s12596-016-0385-7

[4] Ur'Ev E V , Bochkarev E V , Biyalt M A , et al. Study of Torsional Vibrations of Turbomachine Shafts: Part 2. Results of the First Phase Experimental Study of Shafting Torsional Vibrations of a T-175/210-12.75 Turbo Unit. Thermal engineering, 2019, 66(2):84-92.https://doi.org/10.1134/S0040601519010075

[5] Eltaher M A , Agwa M A , Mahmoud F F . Nanobeam sensor for measuring a zeptogram mass. International journal of mechanics and materials in design, 2016, 12(2):211-221.https://doi.org/10.1007/s10999-015-9302-5

[6] Jian Z , Jing S , Bing Z , et al. An Indirect TPMS Algorithm Based on Tire Resonance Frequency Estimated by AR Model. SAE International Journal of Passenger Cars - Mechanical Systems, 2016, 9(1):99-106.https://doi.org/10.4271/2016-01-0459

[7] Mirshafiei F , Mcclure G . Modified three-dimensional seismic assessment method for buildings based on ambient vibration tests: extrapolation to higher shaking levels and measuring the dynamic amplification portion of natural torsion. Earthquake Engineering & Structural Dynamics, 2016, 45(12):2011-2026.https://doi.org/10.1002/eqe.2746

[8] Jain A , Gopal R . Reliability testing of Ni-Fe as structural material in MEMS gyroscope. Journal of micro/nanolithography, MEMS, and MOEMS, 2016, 15(4):040501.1-040501.4.https://doi.org/10.1117/1.JMM.15.4.040501

[9] Maloney L T . Measuring color appearance and the structure of color space. Journal of Vision, 2017, 17(7):30.https://doi.org/10.1167/17.7.30

[10] Zhang L , Kan Y , Meng D , et al. Torsional Vibration Modeling and Analysis of Internal Combustion Engine as a Range Extender. Qiche Gongcheng/automotive Engineering, 2018, 40(9):1101-1109.

[11] Tao Z , Liu X , Guo Q . Torsional vibration model updating for the mill transmission system based on response surface method. Zhendong Ceshi Yu Zhenduan/journal of Vibration Measurement & Diagnosis, 2016, 36(6):1222-1226.

[12] Zhang L , Zhao H , Wang T , et al. Parametric Analysis on Collapse-resistance Performance of Reinforced-concrete Frame with Specially Shaped Columns Under Loss of a Corner Column. The Open Construction and Building Technology Journal, 2016, 10(1):466-480.https://doi.org/10.2174/1874836801610010466

[13] Fogarty J , El-Tawil S . Collapse Resistance of Steel Columns under Combined Axial and Lateral Loading. Journal of structural engineering, 2016, 142(1):04015091.1-04015091.12.https://doi.org/10.1061/(ASCE)ST.1943-541X.0001350

[14] Kitayama S , Constantinou M C . Probabilistic collapse resistance and residual drift assessment of buildings with fluidic self-centering systems. Earthquake Engineering & Structural Dynamics, 2016, 45(12):1935-1953.https://doi.org/10.1002/eqe.2733

[15] Zhang J Z , Li G Q , Jiang J . Collapse resistance of RC beam-slab subassemblies due to column loss at large deflections. Magazine of Concrete Research, 2019, 71(11-12):647-663.https://doi.org/10.1680/jmacr.17.00399

[16] Levasseur T . Decisive Ecological Warfare: Triggering Industrial Collapse via Deep Green Resistance. Journal for the Study of Religion Nature & Culture, 2017, 11(1):109-130.https://doi.org/10.1558/jsrnc.29799

[17] Xue H , Gilbert B P , Guan H , et al. Load Transfer and Collapse Resistance of RC Flat Plates under Interior Column Removal Scenario. Journal of structural engineering, 2018, 144(7):04018087.1-04018087.15.https://doi.org/10.1061/(ASCE)ST.1943-541X.0002090

[18] Han J , Sun X , Zhou Y . Duration effect of spectrally matched ground motion records on collapse resistance capacity evaluation of RC frame structures. The Structural Design of Tall and Special Buildings, 2017, 26(18):e1397.1-e1397.12.https://doi.org/10.1002/tal.1397

[19] Hou J , Song L . Progressive Collapse Resistance of RC Frames under a Side Column Removal Scenario: The Mechanism Explained. International Journal of Concrete Structures and Materials, 2016, 10(2):237-247.https://doi.org/10.1007/s40069-016-0134-y

[20] Li F , Chen F . Seismic collapse resistance of original Class-C frame structure after steel support reinforcement. Liaoning Gongcheng Jishu Daxue Xuebao (Ziran Kexue Ban)/Journal of Liaoning Technical University (Natural Science Edition), 2018, 37(1):92-98.

[21] Huang H , Xian Y , Xi K , et al. Experimental Study and Numerical Analysis on the Progressive Collapse Resistance of SCMS. International journal of steel structures, 2019, 19(1):301-318.https://doi.org/10.1007/s13296-018-0123-x

[22] Fu F , Parke G A R . Assessment of the Progressive Collapse Resistance of Double-Layer Grid Space Structures Using Implicit and Explicit Methods. International Journal of Steel Structures, 2018, 18(3):831-842.https://doi.org/10.1007/s13296-018-0030-1

[23] Khorsandnia N , Valipour H R , Foster S J , et al. Experimental study of progressive collapse resistance of reinforced concrete framed structures. ACI Structural Journal, 2017, 114(6):1385-1396.https://doi.org/10.14359/51689496

[24] Yuan Zhou. Experimental Research of Progressive Collapse Resistance of RC Frame Structure. revista de la facultad de ingenieria, 2016, 31(7):152-161.

[25] Wang T , Zhang L , Zhao H , et al. Progressive collapse resistance of reinforced-concrete frames with specially shaped columns under loss of a corner column. Magazine of Concrete Research, 2016, 68(9):435-449.https://doi.org/10.1680/jmacr.15.00108

[26] Qiu L , Lin F , Wu K . Improving Progressive Collapse Resistance of RC Beam–Column Subassemblages Using External Steel Cables. Journal of Performance of Constructed Facilities, 2020, 34(1):04019079.https://doi.org/10.1680/jmacr.15.00108

[27] Yi-Gang J , Huan L , Guang-Yu W , et al. Spatial nonlinear simulation analysis of progressive collapse resistance of R.C. frame structure under different seismic precautionary. Journal of Intelligent & Fuzzy Systems, 2018, 34(2):1013-1024.https://doi.org/10.3233/JIFS-169395

[28] Bandyopadhyay M , Banik A K . Improvement of progressive collapse resistance potential of semi-rigid jointed steel frames through bracings. International Journal of Protective Structures, 2016, 7(4):518-546.https://doi.org/10.1177/2041419616668085

[29] Rong X , Zhang Q , Zhao Y . Static load experimental research on RC special-shaped columns frame's progressive collapse resistance. World Information on Earthquake Engineering, 2017, 33(2):178-185.

[30] Zhang L , Li H . Experimental study on progressive collapse resistance of steel framed structures. Dongnan Daxue Xuebao, 2018, 48(4):687-691.

[31] Deng K , Lin Y , Liu W , et al. Equations to Calculate Casing Collapse Strength Under Nonuniform Load Based on New ISO Model. Journal of Pressure Vessel Technology, 2016, 138(5):054501.https://doi.org/10.1115/1.4033154